Bioorganic & Medicinal Chemistry Letters 26 (2016) 197–202

Contents lists available at ScienceDirect

Bioorganic & Medicinal Chemistry Letters

journal homepage: www.elsevier.com/locate/bmcl

Fragment-assisted hit investigation involving integrated HTS and fragment screening: Application to the identification of phosphodiesterase 10A (PDE10A) inhibitors

Jeffrey G. Varnes [a,*], Stefan Geschwindner [b], Christopher R. Holmquist [a], Janet Forst [a], Xia Wang [a], Niek Dekker [b], Clay W. Scott [a], Gaochao Tian [a], Michael W. Wood [a], Jeffrey S. Albert [a,*]

[a] CNS Discovery Research, AstraZeneca Pharmaceuticals, 1800 Concord Pike, PO Box 15437, Wilmington, DE 19850-5437, USA
[b] Discovery Sciences, AstraZeneca R&D, SE-431 83 Mölndal, Sweden

ARTICLE INFO

Article history:
Received 4 September 2015
Revised 26 October 2015
Accepted 30 October 2015
Available online 11 November 2015

Keywords:
PDE10A
Fragment-based drug discovery
Fragment-assisted drug discovery
Phosphodiesterase inhibitor
Schizophrenia

ABSTRACT

Fragment-based drug design (FBDD) relies on direct elaboration of fragment hits and typically requires high resolution structural information to guide optimization. In fragment-assisted drug discovery (FADD), fragments provide information to guide selection and design but do not serve as starting points for elaboration. We describe FADD and high-throughput screening (HTS) campaign strategies conducted in parallel against PDE10A where fragment hit co-crystallography was not available. The fragment screen led to prioritized fragment hits (IC_{50}'s ~500 μM), which were used to generate a hypothetical core scaffold. Application of this scaffold as a filter to HTS output afforded a 4 μM hit, which, after preparation of a small number of analogs, was elaborated into a 16 nM lead. This approach highlights the strength of FADD, as fragment methods were applied despite the absence of co-crystallographical information to efficiently identify a lead compound for further optimization.

The cyclic nucleoside monophosphates cAMP and cGMP serve as critical intracellular signaling agents. Signal termination is regulated by hydrolytic cleavage of cAMP and cGMP by members of the phosphodiesterase (PDE) family of enzymes. Among the 11 PDE families, PDE10A has received significant attention as a target for new antipsychotic drugs.[1] PDE10A has a restricted expression pattern within the body, with high levels found only in the brain.[2–4] Specifically, PDE10A protein is localized to the cell bodies and dendrites of the striatal medium spiny neurons (MSN) where it modulates excitability and striatal output.[5,6] These neurons can be separated into two distinct output pathways with different dopamine receptor expression profiles: a D1-expressing 'direct' pathway and a D2-expressing 'indirect' pathway.[7–9]

Clinically validated antipsychotics contain D2 antagonist or partial agonist activity and principally modulate the MSN indirect pathway. However, these medicines do not treat all schizophrenia symptoms (especially negative symptoms and cognitive deficits) and a significant patient population discontinues treatment due to lack of efficacy or the occurrence of adverse effects, indicating significant unmet need.[10] Since PDE10A is expressed in both MSN output pathways, inhibitors of this enzyme offer a novel therapeutic mechanism with a potentially different clinical profile to existing therapy.

Several classes of structurally diverse PDE10A inhibitors from preclinical studies[11] and clinical trials[12] have been described in the literature (Fig. 1). These compounds have resulted from the natural product papavarine (**1**),[1b] random screening and/or structure-based drug design (**2**–**5**),[11–13] and fragment screening.[14] Our strategy to identify novel PDE10A inhibitors was to use alternative screening approaches. We considered using fragment-based drug discovery (FBDD), which is now widely used to identify novel chemotypes,[15–22] however, fragment co-crystallography was not available despite the existence of published and in-house crystallographic data for PDE10A. Instead we chose to use fragment screening information to influence more traditional screening methods, such as high-throughput screening (HTS). This strategy, which is illustrated in Figure 2, is referred to as fragment-*assisted* drug discovery (FADD) to differentiate it from FBDD, where the fragments themselves serve directly as starting points.[18]

An HTS analysis of our corporate compound collection for PDE10A inhibitors afforded more than 11,000 initial hits (>75% PDE10A inhibition, see Supplemental; hit rate: 5%). We eliminated compounds that were structurally related to known PDE inhibitors and those compounds that were of potential risk due to off-target

* Corresponding authors. Tel.: +1 781 839 4944 (J.G.V.), +1 786 529 1730 (J.S.A.).
E-mail addresses: jeffrey.varnes@astrazeneca.com (J.G. Varnes), jeffrey.albert@intellisynrd.com (J.S. Albert).

http://dx.doi.org/10.1016/j.bmcl.2015.10.100
0960-894X/

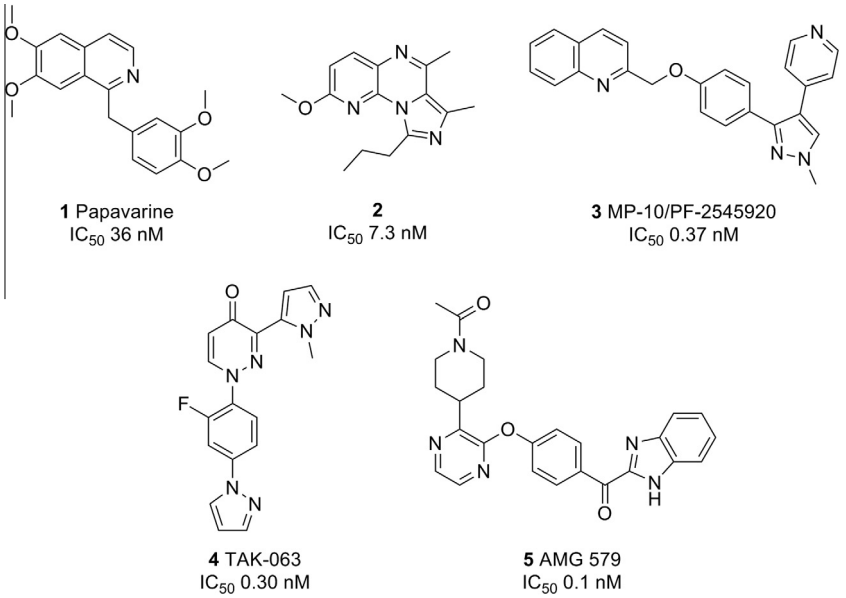

Figure 1. Representative examples of PDE10A inhibitors. Data are reported PDE10A IC_{50}'s according to citations within the text.

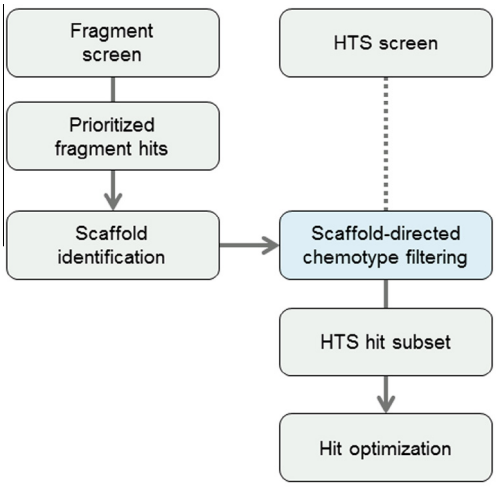

Figure 2. Fragment-assisted drug discovery strategy used to reveal, prioritize, and progress novel PDE10A inhibitors.

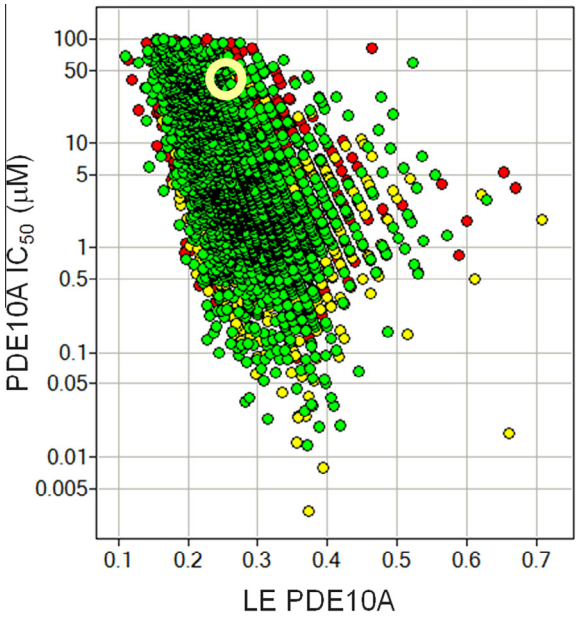

Figure 3. PDE10A inhibition (IC_{50}) versus ligand efficiency[23] (LE). Red: PDE2A-preferring (PDE2A activity >3-fold stronger than PDE10A), yellow: PDE10A-nonselective (PDE2A activity within 3-fold relative to PDE10A), green: PDE10A-preferring (>3-fold stronger than PDE2A activity). The yellow circle indicates the point corresponding to compound **8** according to the original HTS data.

pharmacology, low predicted physical properties, or core pharmacophore features with potentially undesirable metabolic or reactivity profiles. The resulting set of 5328 compounds was tested for multi-dose IC_{50} determination against PDE10A. Additionally, compounds were also analyzed for their activity against PDE2A as an early indication of selectivity. PDE2A was chosen for selectivity profiling among the various isoforms because of its high similarity to PDE10A in the catalytic region, which includes a proximal tyrosine that is analogous to PDE10A's Tyr693.

The results of HTS profiling are shown graphically in Figure 3 where PDE10A IC_{50} (enzyme inhibition assay) is plotted against ligand efficiency[23] (LE) and colored according to PDE2A/PDE10A selectivity ratio. Hits covered a potency range (IC_{50}'s) of 5 nM to 100 μM and were structurally very diverse. In addition, a substantial fraction of compounds had quite high LE; more than 1500 compounds had LE >0.3 and a favorable PDE10A selectivity profile (vs PDE2A).

As part of our alternative screening approach, a fragment screen was conducted in parallel to the HTS on 3000 compounds with low molecular weight (150–250 g/mol and *c*Log*P* −0.8 to 3.0). Fragments were screened at a concentration of 100 μM using OWG (optical waveguide grating) as the detection method to identify hits (>20% PDE10A inhibition) in the 10 μM to 10 mM binding range.[24,25] As with the HTS, the hit rate was quite high (14%) and many compounds (414) had excellent LE (0.30–0.55). Fragment hits (not shown) with the highest LE tended to share certain structural features: they typically were composed of 2 or 3 fused aromatic heterocycles and were reminiscent of **2**.[13] While these were viable starting points, such structures tend to be associated with higher lipophilicity, lower solubility, and possibly reduced druggability.[26]

6
PDE10A IC_{50} 851 μM
LE 0.38

7
PDEA10A IC_{50} 324 μM
LE 0.40

Figure 4. Exemplar biaryl fragment hits with PDE10A activity.

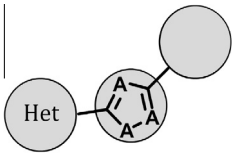

Figure 5. Hypothetical PDE10A scaffold derived from fragment hits **6** and **7** and docking studies where a core five-membered heterocycle is connected to a second heterocycle on one side and an aromatic or hydrophobic group on the other.

A second group of fragment hits, exemplified by heterocycles **6** and **7** (Fig. 4), were fewer in number but had quite different structural features. These compounds had PDE10A binding affinities (IC_{50}'s) of 851 μM and 324 μM, respectively, as measured using a surface plasmon resonance (SPR) binding affinity assay (see Supplemental). Interestingly, since this work was conducted, Hoffman-La Roche has reported several series of PDE10A inhibitors, one of which also contains pyridine–thiazole and pyridine–pyrazole scaffolds.[11g] Other reported scaffolds with similar functionality include Takeda's pyridazinone–pyrazoles (e.g., TAK-063)[12a] and Janssen's imidazopyrazine–pyrazoles.[11a]

To differentiate the potential binding modes of fragment screen hits resembling **2** and those more structurally similar to fragments **6** and **7**, we used computational docking studies (see Supplemental) based on the extensive SAR and structural work discussed by the Pfizer group and others for the class of compounds related to **3**.[11,12] Thus fragment hit **2** was predicted to bind to PDE10A in the region near the catalytic pocket, while **6** and **7** were suggested to bind *between* the selectivity and catalytic pockets. Unfortunately, because we did not have a co-crystal structure for **6** or **7**, both the true position and the orientation of these fragment hits were unknown.

At this stage our objective was to assess how we could use fragment screening results with the previously executed HTS to rapidly identify structurally differentiated lead compounds. Our approach was to select fragments that we considered to be distinct from known PDE10A inhibitors to use as substructure core filters of the extensive HTS hit set. We illustrate this strategy with fragments **6** and **7**, where the absence of a co-crystal structure did not preclude progression since we were looking for novel scaffolds.

We formulated the hypothesis that key structural features of this fragment subset included a core five-membered heterocycle connected to a second heterocycle on one side and an aromatic or hydrophobic group on the other (Fig. 5). We next conducted a bond-connectivity matching analysis of the corporate collection and found that 6000 compounds fit the proposed scaffold; cross-referencing this set with HTS actives led to a 14 compound subset. Of those 14 compounds, 13 were eliminated upon follow-up analysis either because they were false positives or because they contained unattractive functionality. The final compound was benzimidazole **8** (Table 1), which had moderate potency (IC_{50} 3.8 μM) and reasonable LE (0.32). Prompted by this finding we re-screened available close analogs in order to provide some assurance that **8** was not a singleton. Such analogs typically showed weak but detectable activity. For example, **9** showed 23% inhibition of PDE10A activity at 30 μM, which was too weak to establish an IC_{50} (>30 μM). Thus, this small family of weak hits was unremarkable in terms of potency or physical properties. However, we judged that if the compounds did represent elaborated forms of fragment hits **6** and **7** then we might be able to use that knowledge to evolve the chemotype in a more optimal manner.

Starting with **8** as a reference, we explored analogs containing the same benzimidazole–pyrazole left side region and varied the right side amide substituent. A small set of analogs was prepared containing various five- and six-membered aromatic groups. The most potent in the group was **10** (IC_{50} = 0.28 μM). This prompted the evaluation of a set of 2,3-bis-substituted benzamides and led to identification of **11** (IC_{50} = 0.10 μM), which showed high selectivity with respect to PDE2A (IC_{50} >100 μM). Despite this apparent selectivity and high LE (0.38), liabilities included low solubility and increased lipophilicity.

To investigate the role of H-bond donors, we prepared **12**, where the benzimidazole nitrogen was capped by methylation and the pyrazole NH was eliminated by replacing that heterocycle with thiazole. Gratifyingly, **12** showed the highest potency (IC_{50} = 0.016 μM, LE = 0.41) and lowest polar surface area (PSA = 54). Substituents on the aromatic ring of the amide were also revisited in an attempt to decrease lipophilicity. This led to identification of **13** which retained substantial potency (IC_{50} = 0.11 μM, LE = 0.38, *c*Log*P* = 3.3). Subsequent methylation afforded **14**, which was equipotent (IC_{50} = 0.12 μM, LE = 0.36).

We reasoned that since the benzimidazole of **13** could be methylated without potency loss, one of the benzimidazole nitrogens functioned as an acceptor and the other nitrogen had no key interactions with the protein and was likely oriented toward solvent. To test this hypothesis we prepared **15** where the benzimidazole NH was used as a tethering point to add an aminoethyl group as a hydrophilic substituent. This moderately reduced potency and LE (IC_{50} = 0.49 μM, LE = 0.31) but did improve solubility (13 μM) and lipophilicity (*c*Log*P* 2.5). Such improvements in solubility increase the likelihood of generating co-crystal structures and further evolving this chemotype.

The co-crystal structure of **3** with PDE10A as reported by Pfizer is shown in Figure 6.[12c] Two key interactions between **3** (green scaffold) and PDE10A are (1) between the pyrazolopyridine region and the catalytic pocket and (2) between the quinoline and what is termed the selectivity pocket because it is most apparent in PDE10A (and is smaller or absent in other PDE isoforms). This same enzyme structure was used for docking studies with our compounds, and the most favored docked pose for **11** (magenta) is shown overlayed with **3**. According to this model, the benzimidazole nitrogen acts as a hydrogen bond accepter with Tyr693 and thus as a surrogate for the quinoline nitrogen of **3**. This orientation of **11** therefore directs the second benzimidazole nitrogen toward solvent, which is consistent with the observation that there are no significant differences in potency between NH compound **13** (IC_{50} 0.11 μM) and its *N*-methyl analog **14** (IC_{50} 0.12 μM). It is also consistent with the observation that the large aminoethyl replacement in **15** (IC_{50} 0.49 μM) is tolerated, although with reduced potency relative to **13** and **14**. Furthermore, the central pyrazole appears to serve mostly as a spacer and does not contribute any selective binding interactions. Finally, the benzamide aryl group likely participates in a stacking interaction with Phe729.

The synthesis of substituted pyrazoles **8**–**11** is shown Scheme 1, and further details for abbreviations and procedures can be found in Supplemental information. Thus, acid **16**[28] was coupled with 1,2-phenylenediamine using PyClop to afford **17**. Acid-mediated cyclization of this material gave **18**. The nitro group was reduced by catalytic hydrogenation, and the resulting crude amine (**19**) was coupled with an appropriate carboxylic acid prior to deprotection under acidic conditions to afford **8**–**11**.

Table 1
Enzymatic activity and properties of biaryl pyrazoles and analogs

#	Structure	PDE10A IC_{50}[a] (μM)	LE[b]	Sol[c] (μM)	*c*Log*P*	PSA[d]
8	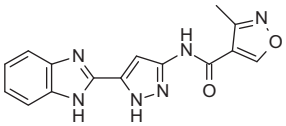	3.8	0.32	2	1.7	107
9	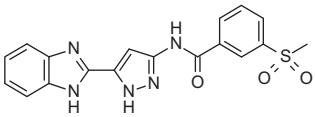	>30	—	nd	2.1	121
10	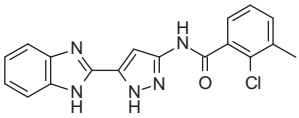	0.28	0.36	<1	3.9	84
11	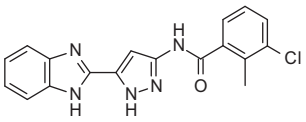	0.10[e,f]	0.38	<1	4.4	84
12	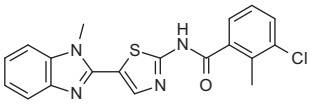	0.016[e,f]	0.41	<1	4.6	54
13	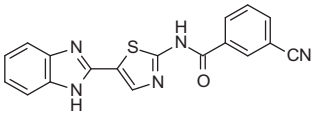	0.11[e,f]	0.38	1	3.3	86
14	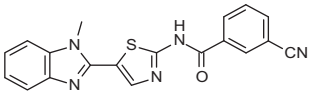	0.12	0.36	<1	3.3	72
15	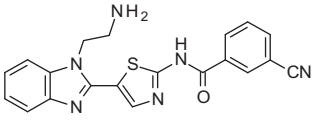	0.49	0.31	13	2.5	100

[a] Results are the average of at least two determinations and reproducibility is <0.3 log units based on replicate determinations.
[b] Ligand efficiency.[23]
[c] Equilibrium solubility at pH 7.4 in phosphate buffer.[27]
[d] Polar surface area.
[e] PDE2A IC_{50} >100 nM.
[f] PDE2A IC_{50} determinations were sometimes made at drug concentrations (in assay buffer) that were higher than the measured equilibrium solubility (at pH 7.4 in phosphate buffer). Test samples were confirmed not to have any visible precipitate, but the drug solubility under the exact assay conditions is unknown and this results in unavoidable uncertainty in assessing PDE2A selectivity.

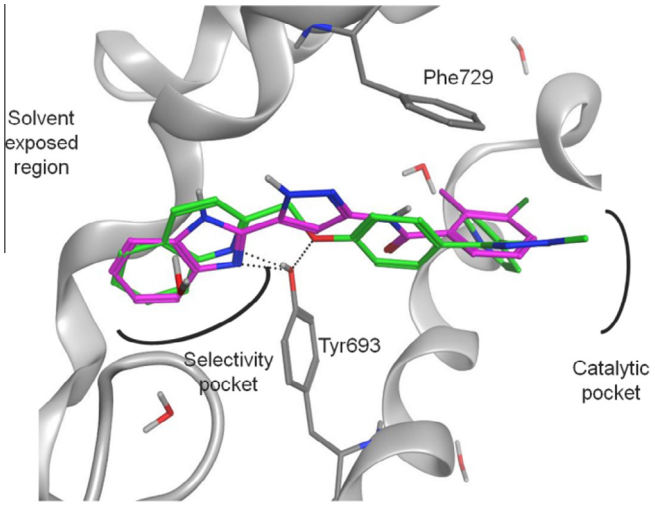

Figure 6. Overlay of the crystallographically determined orientation[12c] of **3** (green) with the computationally derived preferred binding mode of **11** (magenta). Potential hydrogen bond interactions with Tyr693 are shown as dotted lines.

Compounds **12**–**14** (Scheme 2) were prepared by reacting either 5-(1*H*-benzo[*d*]imidazol-2-yl)thiazol-2-amine (**22a**; prepared from commercial **21a**) or 5-(1-methyl-1*H*-benzo[*d*]imidazol-2-yl)thiazol-2-amine[29] (**22b**; prepared from commercial **21b**) with an appropriate benzoic acid and coupling reagent such as TBTU or HATU. Thiazole **15** was prepared from known carbamate **23**[30] following Raney nickel catalyzed hydrogenation to afford **24**, which was cyclized with 2-aminothiazole-5-carbaldehyde to yield **22c**. Acylation of **22c** with 3-cyanobenzyolchloride provided **25**, and deprotection under acidic conditions then gave **15**.

In summary, we employed a high-concentration fragment screen using a biophysical assay. The resulting fragment hits were prioritized based on ligand efficiency, potency, and physical properties. Docking studies suggested that prioritized fragment hits exemplified by **6** and **7** adopted a different binding pose relative to fragments resembling **2**, however, we were unable to co-crystallize the former with the target. While this work was ongoing, we carried out a traditional HTS screen using an enzymatic assay. As expected based on the known high druggability of the target, we observed a high hit rate and, consequently, were left with a large collection of possible starting points.

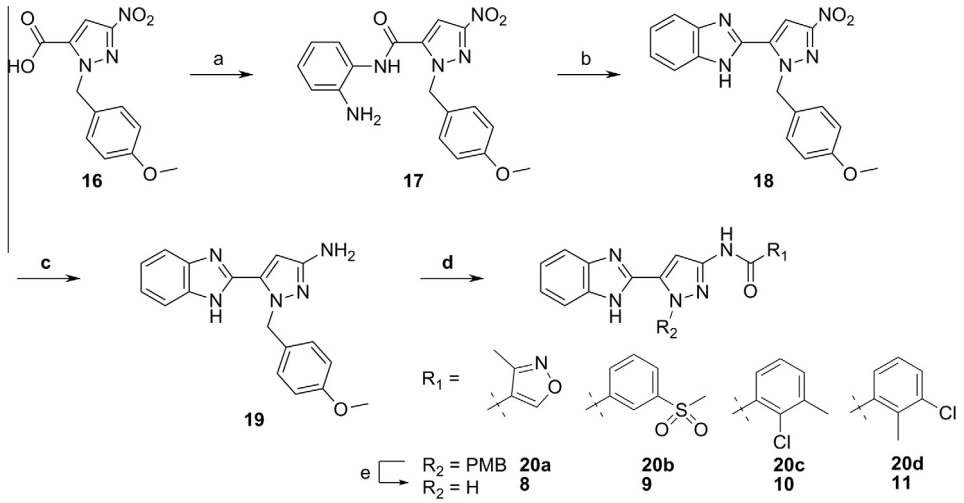

Scheme 1. Reagents and conditions: (a) 1,2-phenylenediamine, PyClop, DIPEA, DCE, 60 °C, 1.5 h, 41%; (b) HOAc, 70 °C, 40 min, 85%; (c) 10% Pd/C, H_2, THF/MeOH, 50 °C, 4 h, 99%; (d) RCO_2H, PyClop, DIPEA, DCE, 60 °C, 4–18 h, 38–85%; (e) TFA, 75 °C, 5 min, 49–86%.

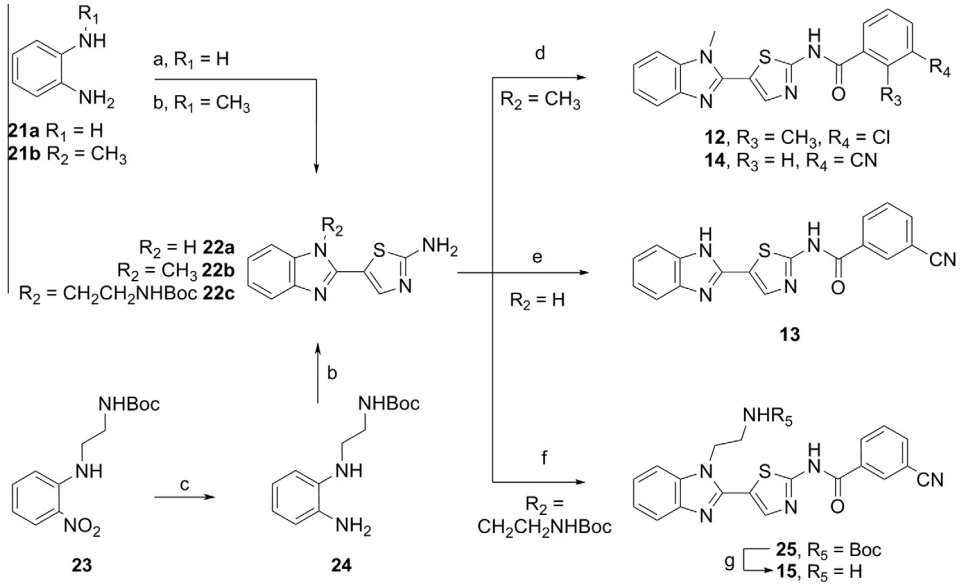

Scheme 2. Reagents and conditions: (a) 2-aminothiazole-5-carbaldehyde, DMSO, 120 °C, 30 h, 63%; (b) 2-aminothiazole-5-carbaldehyde, PEG-400, 110–125 °C, 4 h, 14–64%; (c) Raney Ni, hydrazine, rt, 2 h, 80%; (d) 3-chloro-2-methyl- or 3-cyano-benzoic acid, TBTU, HOBT, DIPEA, DMF, rt, 25–34%; (e) 3-cyanobenzoic acid, HATU, *N*-methylmorpholine, DMF, 60 °C, 18 h, 94%; (f) 3-cyanobenzoyl chloride, DIPEA, DCM, rt, 18 h, 36%; (g) 3 M methanolic HCl, rt, 2 h, 96%.

As an alternative to using fragment hits directly (FBDD), we opted to start with the knowledge derived from our fragment screen (FADD) and hypothesized the key scaffold shown in Figure 5. This scaffold was used to filter our HTS hits, resulting in identification of pyrazole **8** (IC_{50} 3.8 μM). Rapid SAR exploration led to **10** (IC_{50} 0.28 μM), and efforts to reduce the polar surface area (desired PSA: <80) and explore contributions from hydrogen bond donors led to **12** (IC_{50} 0.016 μM), all while retaining good LE. Further exploration led to compounds **14** and **15** which had weaker affinity but modestly better solubility and/or lower *c*Log*P*.

It is unlikely that benzimidazole **8** would have been exploited by HTS data alone simply because of the number of alternative hits and limited resources. This is supported by an assessment of Figure 3, where many hit compounds had stronger potency and higher LE than **8**. Similarly, fragment approaches alone would not have enabled progression of hits **6** and **7** because of their unknown mode of binding and lack of co-crystallization data. Instead, FADD enabled us to apply the benefits of fragment based methods in the absence of fragment co-crystallography to an analysis of an HTS screen and afforded a lead series of PDE10A inhibitors.

Acknowledgements

We gratefully acknowledge the contributions of Helen Feng for the original syntheses of compounds **8**–**11**. We also acknowledge Camil Joubran and Nancy Degrace for confirming the structures of **17** and **18**.

Supplementary data

Supplementary data associated with this article can be found, in the online version, at http://dx.doi.org/10.1016/j.bmcl.2015.10.100.

References and notes

1. (a) Wilson, L. S.; Brandon, N. J. *Curr. Pharm. Des.* **2015**, *21*, 378; (b) Siuciak, J. A. *CNS Drugs* **2008**, *22*, 983.
2. Fujishige, K.; Kotera, J.; Omori, K. *Eur. J. Biochem.* **1999**, *266*, 1118.
3. Fujishige, K.; Kotera, J.; Michibata, H.; Yuasa, K.; Takebayashi, S.; Okumura, K.; Omori, K. *J. Biol. Chem.* **1999**, *274*, 18438.
4. Loughney, K.; Snyder, P. B.; Uher, L.; Rosman, G. J.; Ferguson, K.; Florio, V. A. *Gene* **1999**, *234*, 109.
5. Soderling, S. H.; Bayuga, S. J.; Beavo, J. A. *Proc. Natl. Acad. Sci. U.S.A.* **1999**, *96*, 7071.
6. Coskran, T. M.; Morton, D.; Menniti, F. S.; Adamowicz, W. O.; Kleiman, R. J.; Ryan, A. M.; Strick, C. A.; Schmidt, C. J.; Stephenson, D. T. *J. Histochem. Cytochem.* **2006**, *54*, 1205.
7. Graybiel, A. M. *Curr. Biol.* **2000**, *10*, R509.
8. Graybiel, A. M. *Trends Neurosci.* **1990**, *13*, 244.
9. Surmeier, D. J.; Ding, J.; Day, M.; Wang, Z.; Shen, W. *Trends Neurosci.* **2007**, *30*, 228.
10. Lieberman, J. A.; Stroup, T. S.; McEvoy, J. P.; Swartz, M. S.; Rosenheck, R. A.; Perkins, D. O.; Keefe, R. S.; Davis, S. M.; Davis, C. E.; Lebowitz, B. D.; Severe, J.; Hsiao, J. K. *N. Eng. J. Med.* **2005**, *353*, 1209.
11. For recent literature on preclinical PDE10A inhibitors, see: (a) Bartolomé-Nebreda, J. M.; Alonso de Diego, S. A.; Artola, M.; Delgado, F.; Delgado, O.; Martín-Martín, M. L.; Martínez-Viturro, C. M.; Pena, M. A.; Tong, H. M.; Van Gool, M.; Alonso, J. M.; Fontana, A.; Macdonald, G. J.; Megens, A.; Langlois, X.; Somers, M.; Vanhoof, G.; Conde-Ceide, S. *J. Med. Chem.* **2015**, *58*, 978; (b) Burdi, D. F.; Campbell, J. E.; Wang, J.; Zhao, S.; Zhong, H.; Wei, J.; Campbell, U.; Shao, L.; Koch, P.; Jones, P. G.; Hewitt, M. C. *Bioorg. Med. Chem. Lett.* **2015**, *25*, 1864; (c) Das, S.; Harde, R. L.; Shelke, D. E.; Khairatkar-Joshi, N.; Bajpai, M.; Sapalya, R. S.; Surve, H. V.; Gudi, G. S.; Pattem, R.; Behera, D. B.; Jadhav, S. B.; Thomas, A. *Bioorg. Med. Chem. Lett.* **2014**, *24*, 2073; (d) Kilburn, J. P.; Kehler, J.; Langgard, M.; Erichsen, M. N.; Leth-Petersen, S.; Larsen, M.; Christoffersen, C. T.; Nielsen, J. *Bioorg. Med. Chem.* **2013**, *21*, 6053; (e) Yang, S.-W.; Smotryski, J.; McElroy, W. T.; Tan, Z.; Ho, G.; Tulshian, D.; Greenlee, W. J.; Guzzi, M.; Zhang, X.; Mullins, D.; Xiao, L.; Hruza, A.; Chan, T.-M.; Rindgen, D.; Bleickardt, C.; Hodgson, R. *Bioorg. Med. Chem. Lett.* **2012**, *22*, 235; (f) McElroy, W. T.; Tan, Z.; Basu, K.; Yang, S.-W.; Smotryski, J.; Ho, G. D.; Tulshian, D.; Greenlee, W. J.; Mullins, D.; Guzzi, M.; Zhang, X.; Bleickardt, C.; Hodgson, R. *Bioorg. Med. Chem. Lett.* **2012**, *22*, 1335; For reviews of PDE10A literature prior to 2012, see the following and references therein: (g) Chappie, T. A.; Helal, C. J.; Xinjun, H. *J. Med. Chem.* **2012**, *55*, 7299.
12. See the following papers and references therein for representative compounds that have progressed into the clinic for PDE10A inhibition: Takeda, TAK-063: (a) Kunitomo, J.; Yoshikawa, M.; Fushimi, M.; Kawada, A.; Quinn, J. F.; Oki, H.; Kokubo, H.; Kondo, M.; Nakashima, K.; Kamiguchi, N.; Suzuki, K.; Kimura, H.; Taniguchi, T. *J. Med. Chem.* **2014**, *57*, 9627; Amgen, AMG 579: (b) Hu, E.; Chen, N.; Bourbeau, M. P.; Harrington, P. E.; Biswas, K.; Kunz, R. K.; Andrews, K. L.; Chmait, S.; Zhao, X.; Davis, C.; Ma, J.; Shi, J.; Lester-Zeiner, D.; Danao, J.; Able, J.; Cueva, M.; Talreja, S.; Kornecook, T.; Chen, H.; Porter, A.; Hungate, R.; Treanor, J.; Allen, J. R. *J. Med. Chem.* **2014**, *57*, 6632; Pfizer, PF-02545920/MP-10: (c) Verhoest, P. R.; Chapin, D. S.; Corman, M.; Fonseca, K.; Harms, J. F.; Hou, X.; Marr, E. S.; Menniti, F. S.; Nelson, F.; O'Connor, R.; Pandit, J.; Proulx-LaFrance, C.; Schmidt, A. W.; Schmidt, C. J.; Suiciak, J. A.; Liras, S. *J. Med. Chem.* **2009**, *52*, 5188; (d) Roche, RG-7203, For a representative patent, see: Alberati, D.; Sanchez, R. A.; Bleicher, K.; Flohr, A.; Zbinben, K. G.; Koerner, M.; Kuhn, B.; Peters, J. -U.; Rudolph, M. US 2011/0071128 A1, 2011.
13. Hofgen, N.; Stange, H.; Schindler, R.; Lankau, H. J.; Grunwald, C.; Langen, B.; Egerland, U.; Tremmel, P.; Pangalos, M. N.; Marquis, K. L.; Hage, T.; Harrison, B. L.; Malamas, M. S.; Brandon, N. J.; Kronbach, T. *J. Med. Chem.* **2010**, *53*, 4399.
14. Law, R.; Barker, O.; Barker, J. J.; Hesterkamp, T.; Godemann, R.; Andersen, O.; Fryatt, T.; Courtney, S.; Hallett, D.; Whittaker, M. *J. Comput. Aided Mol. Des.* **2009**, *23*, 459.
15. (a) Chessari, G.; Woodhead, A. *Drug Discovery Today* **2009**, *14*, 668; (b) Murray, C. W.; Rees, D. C. *Nat. Chem.* **2009**, *1*, 187.
16. Pellecchia, M. *Nat. Chem. Biol.* **2009**, *5*, 274.
17. Schulz, M. N.; Hubbard, R. E. *Curr. Opin. Pharmacol.* **2009**, *9*, 615.
18. (a) Whittaker, M. *Drug Discovery Today* **2009**, *14*, 623; For examples of FADD in industry, see also: (b) Lepre, C. *Expert Opin. Drug Discov.* **2007**, *2*, 1555; (c) Whittaker, M.; Law, R. J.; Ichihara, O.; Hesterkamp, T.; Hallett, D. *Drug Discovery Today* **2010**, *7*, 163; (d) Heifetz, A.; Mazanetz, M.; James, T.; Pal, S.; Law, R. J.; Slack, M.; Biggin, P. C. *Med. Chem.* **2013**, *4*, 313; (e) Cheney, D. L.; Bozarth, J. M.; Metzler, W. J.; Morin, P. E.; Mueller, L.; Newitt, J. A.; Nirschl, A. H.; Rendina, A. R.; Tamura, J. K.; Wei, A.; Wen, X.; Wurtz, N. R.; Seiffert, D. A.; Wexler, R. R.; Priestley, E. S. *J. Med. Chem.* **2015**, *58*, 2799.
19. de Kloe, G. E.; Bailey, D.; Leurs, R.; de Esch, I. J. *Drug Discovery Today* **2009**, *14*, 630.
20. Congreve, M.; Chessari, G.; Tisi, D.; Woodhead, A. J. *J. Med. Chem.* **2008**, *51*, 3661.
21. Zartler, E. R.; Shapiro, M. J. *Fragment-Based Drug Discovery: A Practical Approach*; Wiley: Chichester, 2008.
22. (a) Hajduk, P. J.; Greer, L. *Nat. Rev. Drug Disc.* **2007**, *6*, 211; (b) Jahnke, W.; Erlanson, D. A. *Fragment-Based Approaches to Lead Discovery*; Wiley: Weinheim, 2007.
23. LE = $-RT(\ln(IC_{50}))/(\text{heavy atom count})$.
24. Geschwindner, S.; Dekker, N.; Horsefield, R.; Tigerström, A.; Johannson, P.; Scott, C. W.; Albert, J. S. *J. Med. Chem.* **2013**, *56*, 3228.
25. Geschwindner, Stefan Methods in Pharmacology and Toxicology. In *Part II: Label-Free Biosensor Methods in Drug Discovery*; Fang, Y., Ed.; Springer: New York, 2015; pp 119–132.
26. Lovering, F.; Bikker, J.; Humblet, C. *J. Med. Chem.* **2009**, *52*, 6752.
27. Alelyunas, Y. W.; Liu, R.; Pelosi-Kilby, L.; Shen, C. *Eur. J. Pharm. Sci.* **2009**, *37*, 172.
28. Rzepecki, P.; Wehner, M.; Molt, O.; Zadmard, R.; Harms, K.; Schrader, T. *Synthesis* **2003**, 1815.
29. Mukhopadhyay, C.; Tapaswi, P. K. *Tetrahedron Lett.* **2008**, *49*, 6237.
30. Cole, D. C.; Bernotas, R. C. US, 020575, 2005.